Architecture of TOI-561 planetary system

Citation for the original published paper (version of record):
Piotto, G., Zingales, T., Borsato, L. et al (2024). Architecture of TOI-561 planetary system. Monthly Notices of the Royal Astronomical Society, 535(3): 2763-2774.
http://dx.doi.org/10.1093/mnras/stae2440

Monthly Notices of the ROYAL ASTRONOMICAL SOCIETY

MNRAS **535,** 2763–2774 (2024) https://doi.org/10.1093/mnras/stae2440
Advance Access publication 2024 November 21

Architecture of TOI-561 planetary system

G. Piotto [1,2] T. Zingales [1,2★] L. Borsato [2] J. A. Egger,[3] A. C. M. Correia [4] A. E. Simon,[3,5] H.-G. Florén,[6] S. G. Sousa [7] P. F. L. Maxted [8] D. Nardiello [1,2] L. Malavolta [1,2] T. G. Wilson [9] Y. Alibert,[3,5] V. Adibekyan,[7] A. Bonfanti,[10] R. Luque [11] N. C. Santos,[7,12] M. J. Hooton,[13] L. Fossati,[10] A. M. S. Smith,[14] S. Salmon,[15] G. Lacedelli,[16] R. Alonso,[16,17] T. Bárczy,[18] D. Barrado Navascues,[19] S. C. C. Barros,[7,12] W. Baumjohann,[10] T. Beck,[3] W. Benz,[3,5] N. Billot,[15] A. Brandeker,[6] C. Broeg,[3,5] M. Buder,[14] A. Collier Cameron [20] Sz. Csizmadia [14] P. E. Cubillos,[10,21] M. B. Davies,[22] M. Deleuil,[23] A. Deline,[15] O. D. S. Demangeon,[7,12] B.-O. Demory,[3,5] A. Derekas,[24] B. Edwards,[25] D. Ehrenreich,[15,26] A. Erikson,[14] A. Fortier,[3,5] M. Fridlund,[27,28] D. Gandolfi [29] K. Gazeas,[30] M. Gillon,[31] M. Güdel,[32] M. N. Günther [33] A. Heitzmann,[15] Ch. Helling,[10,34] K. G. Isaak,[33] L. L. Kiss,[35,36] J. Korth,[37] K. W. F. Lam [14] J. Laskar,[38] A. Lecavelier des Etangs,[39] M. Lendl [15] P. Leonardi,[1,40] D. Magrin,[2] G. Mantovan [1,2] C. Mordasini,[3,5] V. Nascimbeni [2] G. Olofsson,[6] R. Ottensamer,[32] I. Pagano,[41] E. Pallé,[16,17] G. Peter,[42] R. Ottensamer,[43] D. Pollacco,[9] D. Queloz,[13,44] R. Ragazzoni,[1,2] N. Rando,[33] F. Ratti,[33] H. Rauer,[14,45] I. Ribas,[46,47] G. Scandariato,[41] D. Ségransan,[15] D. Sicilia,[48] M. Stalport,[31,49] S. Sulis,[23] Gy. M. Szabó,[24,50] S. Udry,[15] S. Ulmer-Moll,[5,10,49] V. Van Grootel,[49] J. Venturini,[15] E. Villaver,[16,17] N. A. Walton[13], J. N. Winn[43] and S. Wolf[15]

Affiliations are listed at the end of the paper

Accepted 2024 October 22. Received 2024 October 21; in original form 2024 August 8

ABSTRACT

We present new observations from *CHEOPS (CHaracterising ExOPlanet Satellite)* and *TESS (Transiting Exoplanet Survey Satellite)* to clarify the architecture of the planetary system hosted by the old Galactic thick disc star TOI-561. Our global analysis, which also includes previously published photometric and radial velocity data, incontrovertibly proves that TOI-561 is hosting at least four transiting planets with periods of 0.44 d (TOI-561 b), 10.8 d (TOI-561 c), 25.7 d (TOI-561 d), and 77.1 d (TOI-561 e) and a fifth non-transiting candidate, TOI-561f with a period of 433 d. The precise characterization of TOI-561's orbital architecture is interesting since old and metal-poor thick disc stars are less likely to host ultrashort-period super-Earths like TOI-561 b. The new period of planet -e is consistent with the value obtained using radial velocity alone and is now known to be 77.14399 ± 0.00025 d, thanks to the new *CHEOPS* and *TESS* transits. The new data allowed us to improve its radius ($R_p = 2.517 \pm 0.045\,R_\oplus$ from 5 per cent to 2 per cent precision) and mass ($M_p = 12.4 \pm 1.4\,M_\oplus$) estimates, implying a density of $\rho_p = 0.778 \pm 0.097\,\rho_\oplus$. Thanks to recent *TESS* observations and the focused *CHEOPS* visit of the transit of TOI-561 e, a good candidate for exomoon searches, the planet's period is finally constrained, allowing us to predict transit times through 2030 with 20-min accuracy. We present an updated version of the internal structure of the four transiting planets. We finally performed a detailed stability analysis, which confirmed the long-term stability of the outer planet TOI-561 f.

Key words: techniques: photometric – techniques: radial velocities – ephemerides – planets and satellites: dynamical evolution and stability – planets and satellites: fundamental parameters – planets and satellites: interiors.

1 INTRODUCTION

The planetary system orbiting the old Galactic thick disc star TOI-561 is currently known to include an ultrashort-period (USP) planet and at least three mini-Neptunes. There has been controversy in the literature over the correct architecture of this system. It represents a sort of unique situation in which the analysis of the same light curves and two radial velocity (RV) data sets led to two different solutions, in disagreement regarding the number of planets in the system, their masses, and even their periods (Lacedelli et al. 2021, 2022; Weiss et al. 2021).

More recently, Lacedelli et al. (2022) detected a further planet candidate with a period of about 400 d based on the High Accuracy Radial velocity Planet Searcher for the Northern hemisphere (HARPS-N) RV data. The existence of this fifth non-

★ E-mail: tiziano.zingales@unipd.it

Table 1. *CHEOPS* observations of TOI-561 system. Each row provides the time window of the observation, with the starting and the end time of each visit, the *CHEOPS* data name, and the planets that fall into the specific visit.

Start [UTC]	End [UTC]	Duration [h]	Number of frames	Integration time [s]	File key	Planet
2022-02-06 23:54	2022-02-08 06:03	30.16	1179	60	CH_PR100031_TG049101_V0200	b,e
2021-04-12 23:52	2021-04-15 05:37	53.76	2057	60	CH_PR100031_TG039301_V0200	b,d
2021-03-29 10:19	2021-03-29 14:44	4.42	212	60	CH_PR100008_TG000811_V0200	b,c
2021-01-23 15:29	2021-01-24 07:09	15.67	617	60	CH_PR100031_TG037001_V0200	b,c

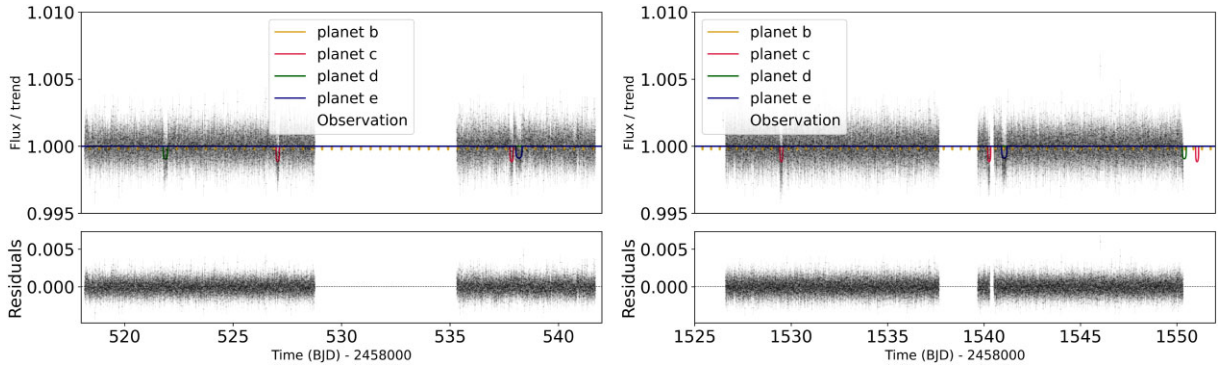

Figure 1. TOI-561 *TESS* observations. Different colours show the light curve of the different transiting planet models. Left: *TESS* Sector 8 with PYORBIT models. Right: *TESS* Sector 45 with the PYORBIT models.

transiting planet needs to be confirmed with future observational surveys.

In this work, based on additional *TESS* (Ricker et al. 2015) and *CHEOPS* (Benz et al. 2021; Fortier et al. 2024), data, we confirm that TOI-561 is a system made of five planets, four of which have been detected by transits. Its host star is one of the oldest objects in our Galaxy ($t_* = 11.0^{+2.8}_{-3.5}$ Gyr, Lacedelli et al. 2022) with a detected planetary system. TOI-561 is one of the 78.[1] Planetary systems with at least four confirmed exoplanets and a USP planet. Refining the planetary structure and orbital configuration will open a window about the earlier planetary formation and evolution in our Galaxy. TOI-561 b stands out as a USP with extremely low density. TOI-561 b seems to have lost most of its atmosphere and might host water. For further details on the structure of TOI-561 b, see Patel et al. (2023). This planet was selected among the winning *JWST* Proposals in Cycle 2, ID no. 3860, PI: J. Teske.

Usually, young, slow, and metal-rich stars associated with the thin disc host averagely more exoplanets, especially close-in super-Earths (Bashi & Zucker 2021). It means that the TOI-561 exoplanetary system is very peculiar since it is unlikely for an old and metal-poor thick disc star to host a USP. Considering the properties of this system, the USP TOI-561 b is likely composed of high mean molecular weight species (Brinkman et al. 2022).

TOI-561 f is the only non-transiting candidate exoplanet in this system. RV data suggest an orbital period of over 400 d. Correct knowledge of the properties of this fifth planet are very important to constrain the dynamics and formation mechanisms of planets around old stars like TOI-561. Its existence also raises interesting questions about the possibility of other transiting and non-transiting planets in the system that could be identified with long-term follow-up and more advanced methods.

The fourth transiting planet, TOI-561 e was first inferred from HARPS-N RV. The ephemerides obtained from the RVs allowed Lacedelli et al. (2021) to identify a corresponding transit of the $\sim$ 77 d period planet in *TESS* Sector 8. The values shown in Lacedelli et al. (2021) helped us detect a new transit in Sector 45, which was indeed observed and visible in the TESS Image CAlibrator (TICA) full frame images (FFIs) of this sector. With the use of the new ephemerides, we scheduled an observation of the TOI-561 system using the *CHEOPS* telescope. In this work, we present the refined ephemerides and the new planetary architecture of the TOI-561 system using the newest *CHEOPS* + *TESS* observations. We confirm the presence of the fourth transiting planet, clarifying the architecture of the system, and we present new ephemerides and analysis of the structure of the planets orbiting TOI-561. Because of its long period, TOI-561 e is one of the few good candidates for the search for exomoons and, therefore, suited for follow-up.

In Section 2, we describe all the new observations. In Section 3, we show the final analysis performed for this system, highlighting the improvement of the ephemerides of all targets (Section 4). In Section 5, we perform a stability analysis of TOI-561 f's orbit, the outermost candidate exoplanet of this system. Finally, we show an improved internal structure model for all the transiting exoplanets (Section 6).

2 OBSERVATIONS

We extracted the light curve of TOI-561 from the TICA[2] (Fausnaugh et al. 2021) images collected during Sector 45 (from 2021 November 06 to December 02). For the light-curve extraction, we used the PATHOS pipeline developed by Nardiello et al. (2019) and Nardiello (2020) adapted to TICA images. Light curves were corrected by applying to them Cotrending Basis Vectors obtained as in Nardiello et al. (2020).

The TICA analysis of Sector 45 made it possible to refine the ephemerides and schedule a further transit of planet TOI-561 e with

[1] https://exoplanetarchive.ipac.caltech.edu/

[2] https://archive.stsci.edu/hlsp/tica

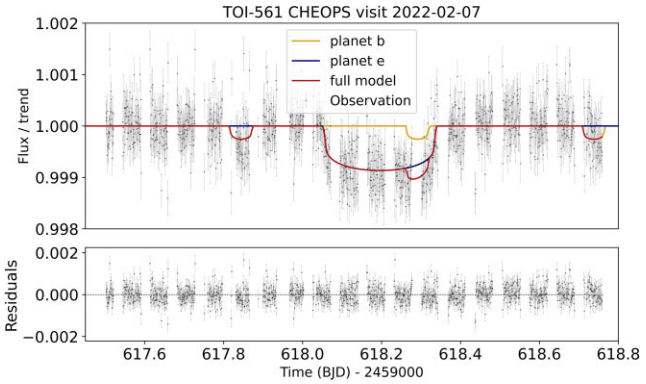

Figure 2. TOI-561 light curve from *CHEOPS* last visit of 2022 February 7.

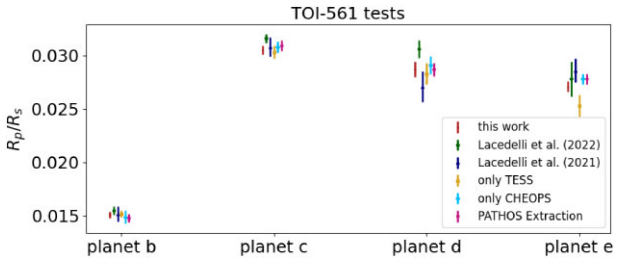

Figure 3. Comparison in the R_p/R_* ratio for all the tests made in this letter. The figure illustrates the results obtained using only *TESS* data, only *CHEOPS* data, and from the independent analysis made by extracting *TESS* light curves with the PATHOS code.

CHEOPS on 2022 February 7. We used four *CHEOPS* observations of the TOI-561 system that cover the transits of planets b, c, d, and e, from 2021 January 23 to 2022 February 08 (see Table 1 for a chronology of the observations).

Additionally, we used *TESS* FFIs of Sectors 46 (from 2021 December 02 to 30) and 72 (from 2023 November 11 to December 07). We extracted the raw light curves from FFIs by using the PYPATHOS pipeline (see Nardiello et al. 2019, 2021) and we corrected them by applying the cotrending basis vectors obtained by Nardiello et al. (2020).

We used the published RVs of TOI-561, which have been obtained with HARPS-N at the Telescopio Nazionale Galileo (Cosentino et al. 2014), and HIRES (High Resolution Echelle Spectrometer) at Keck (Vogt & Keane 1993), for a total of 122 and 61 RV measurements, respectively. We refer to Lacedelli et al. (2021, 2022) and Weiss et al. (2021) for more details on spectroscopic data.

3 PHOTOMETRIC AND RV ANALYSIS

We used the light curves delivered by the *CHEOPS* Data Reduction Pipeline (DRP v13, Hoyer et al. (2020)). The *CHEOPS* DRP automatically calibrates and corrects the data and delivers the photometric light curves obtained with different aperture sizes. In this work, we used the DEFAULT ($R = 25$) aperture which has the best light curve in terms of dispersion. *CHEOPS* observations have been detrended using CHEOPE,[3] a PYTHON tool which uses PYCHEOPS (Maxted et al. 2021) as a backend and optimized to extract the planetary signal from the *CHEOPS* data frames. CHEOPE uses `lmfit` (Newville et al. 2014) to select the best detrending models and the EMCEE (Foreman-Mackey et al. 2013) package for the Bayesian framework. All *CHEOPS* light curves from Lacedelli et al. (2021, 2022), including the one from the last *CHEOPS* visit of TOI-561 e, were re-analysed with CHEOPE.

We used the PDCSAP (Pre-search Data Conditioning Simple Aperture Photometry)*TESS* light curves (Fig. 1) from Sectors 8, 35, 45, 46, and 72 and flattened using `wotan` (Hippke et al. 2019), which allow to model the stellar flux with a Tukey's biweight estimator (Mosteller & Tukey 1977).

The stellar radius was computed using the method described in Lacedelli et al. (2022). They used a Markov Chain Monte Carlo (MCMC) Infrared flux method (IRFM) method that compares broadband photometry to stellar spectral catalogues using the results of their spectral analysis, such as metallicity, as priors. Thanks to *Gaia* contribution with improved parallaxes and distances, we can now get down to 1 per cent (internal) stellar radius uncertainties. This can also be seen in independent works using the ARIADNE code.[4,5]

To obtain an updated architecture of the TOI-561 system, we performed a simultaneous modelling of all available photometric data from *CHEOPS* and *TESS*, and spectroscopic data from HARPS-N and HIRES. We used the code PYORBIT (Malavolta et al. 2016, 2018) with the PYDE+EMCEE sampling method (Foreman-Mackey et al. 2013; Parviainen 2016). To find the best starting point for the MCMC sampling, we used PYDE with 64 000 generators on our data sets. Then, we ran 100 chains for 150 000 steps, discarding the first 40 000 and applying a thinning factor of 100. We used the same priors and boundaries as reported in Lacedelli et al. (2022) unless otherwise specified in this section.

We assumed four transiting planets plus a fifth non-transiting Keplerian applying a uniform prior on the period between 2 and 1000 d. We used the same stellar parameters as described in Lacedelli et al. (2022). The limb darkening has been parametrized using the quadratic law, as described in Kipping (2013), using Gaussian priors on the u_1 and u_2 coefficients, computed for both *CHEOPS* and *TESS* passbands, adopting a bilinear interpolation of the limb-darkening profile as defined in Claret (2017, 2021). The RV data points in this analysis are the same used in Lacedelli et al. (2022), so we do not report any significant change in the RV semi-amplitude and, then, on the masses of the planets.

To exclude that our detrending was affecting the results, we also performed an independent global analysis with the JULIET package (Espinoza, Kossakowski & Brahm 2019) including all the available data sets and fitting all the planetary models simultaneously. The results from PYORBIT and JULIET were consistent with each other, indicating that our assumptions and detrending did not significantly affect the results of our analysis.

During the last visit with *CHEOPS*, also the USP planet TOI-561 b was transiting in front of the star. The simultaneous fit of PYORBIT allows us to distinguish the two components of this transit (Fig. 2).

The new analysis, using latest new photometric data, improves our knowledge of the orbital parameters of the four transiting planets, i.e. TOI-561 b ($P = 0.4465697 \pm 0.0000003$ d and $R_p = 1.397 \pm 0.027\,R_\oplus$), c ($P = 10.778838 \pm 0.000018$ d and $R_p = 2.865 \pm 0.041\,R_\oplus$), d ($P = 25.71268 \pm 0.00012$ d and $R_p = 2.615 \pm 0.059\,R_\oplus$), and e ($P = 77.14400 \pm 0.00027$ d and $R_p = 2.517 \pm 0.045\,R_\oplus$) and refutes the existence of the planet at $P = 16.3$ d found in Weiss et al. (2021).

[3] https://github.com/tiziano1590/cheops_analysis-package

[4] https://arxiv.org/abs/2204.03769,

[5] https://github.com/jvines/astroARIADNE)

Table 2. Parameters for the TOI-561 planetary system.

	Planetary parameters				
	TOI-561 b	TOI-561 c	TOI-561 d	TOI-561 e	5th Keplerian
P [d]	0.4465697 ± 0.0000003	10.778838 ± 0.000018	25.71268 ± 0.00012	77.14400 ± 0.00027	433^{+20}_{-18}
T_0[TBJD][a]	2317.75002 ± 0.00041	2238.46284 ± 0.00079	2318.9711 ± 0.0021	1538.1803 ± 0.0035	–
a/R_*	2.683 ± 0.029	22.40 ± 0.25	40.00 ± 0.44	83.21 ± 0.91	$262.9^{+8.5}_{-7.9}$
a [au]	0.01064 ± 0.00016	0.0889 ± 0.0013	0.1587 ± 0.0024	0.3300 ± 0.0050	1.043 ± 0.035
R_p/R_*	0.01519 ± 0.00028	0.03115 ± 0.00041	0.02842 ± 0.00063	0.02736 ± 0.00047	–
R_p [$R_\oplus$]	1.397 ± 0.027	2.865 ± 0.041	2.615 ± 0.059	2.517 ± 0.045	–
b	$0.14^{+0.096}_{-0.094}$	$0.15^{+0.14}_{-0.10}$	$0.36^{+0.13}_{-0.19}$	$0.19^{+0.14}_{-0.13}$	–
i [deg]	$87.0^{+2.0}_{-2.1}$	$89.61^{+0.27}_{-0.33}$	$89.51^{+0.25}_{-0.14}$	$89.864^{+0.095}_{-0.094}$	–
T_{14} [d]	0.05452 ± 0.00066	$0.1558^{+0.0022}_{-0.0042}$	0.197 ± 0.012	$0.2974 \pm^{+0.0057}_{-0.01}$	–
e	0 (fixed)	$0.023^{+0.034}_{-0.017}$	$0.111^{+0.050}_{-0.039}$	$0.074^{+0.044}_{-0.039}$	$0.083^{+0.080}_{-0.058}$
ω [deg]	90 (fixed)	219^{+87}_{-149}	-131^{+17}_{-26}	148^{+26}_{-39}	-66^{+66}_{-83}
K[m s^{-1}]	1.95 ± 0.21	1.98 ± 0.21	3.36 ± 0.22	2.16 ± 0.23	1.88 ± 0.25
M_p [$M_\oplus$][b]	2.02 ± 0.23	5.93 ± 0.67	13.33 ± 0.98	12.4 ± 1.4	19.1 ± 2.7
ρ_p [$\rho_\oplus$]	0.741 ± 0.095	0.252 ± 0.030	0.745 ± 0.074	0.778 ± 0.097	–
ρ_p [g cm^{-3}]	4.1 ± 0.5	1.3 ± 0.2	4.1 ± 0.4	4.3 ± 0.5	–
T_{eq}[K][c]	2319 ± 34	802 ± 12	600 ± 9	$416 \pm 6\,234 \pm 5$	
S_p [$S_\oplus$][d]	4709 ± 153	67.5 ± 2.2	21.2 ± 0.7	4.89 ± 0.16	0.49 ± 0.03
g_p^e [m s^{-2}]	10.1 ± 1.2	7.1 ± 0.8	19.1 ± 1.6	19.2 ± 2.3	–
	Common parameters				
R_*^f [$R_\odot$]	0.843 ± 0.005				
M_*^f [$M_\odot$]	0.806 ± 0.036				
ρ_*[$\rho_\odot$]	1.31 ± 0.05				
$u_{1,\mathrm{TESS}}$	0.33 ± 0.08				
$u_{2,\mathrm{TESS}}$	0.23 ± 0.09				
$u_{1,\mathrm{CHEOPS}}$	0.46 ± 0.07				
$u_{2,\mathrm{CHEOPS}}$	0.22 ± 0.09				
$\sigma^g_{\mathrm{HARPS-N}}$ [m s^{-1}]	1.35 ± 0.16				
$\sigma^g_{\mathrm{HIRES}}$ [m s^{-1}]	2.84 ± 0.36				
$\gamma^h_{\mathrm{HARPS-N}}$ [m s^{-1}]	79699.32 ± 0.25				
$\gamma^h_{\mathrm{HIRES}}$ [m s^{-1}]	-1.27 ± 0.42				

Notes. [a] *TESS* Barycentric Julian Date (BJD – 2457000). [b] Minimum mass in the hypothesis of a planetary origin. [c] Computed as $T_{\mathrm{eq}} = T_* \left(\frac{R_*}{2a}\right)^{1/2} [(1 - A_b)]^{1/4}$, assuming null Bond albedo ($A_b = 0$). [d] Stellar irradiation at the surface. [e] Planetary surface gravity. [f] As determined from the stellar analysis in Lacedelli et al. (2022). [g] RV jitter term. [h] RV offset.

Our analysis resulted in an improvement of the radius of TOI-561 e with an error reduced to 2 per cent, thanks to the new *TESS+CHEOPS* observations. For comparison, in Lacedelli et al. (2022), the precision on the radius was 5 per cent. Lacedelli et al. (2022) have a precision on P_e of about 6 h, while in this work we reached a precision of 21.6 s.

In order to resolve the discrepancies appearing in the values of R_p/R_* for TOI-561 c and d as reported by Lacedelli et al. (2022), we performed three different tests in an independent manner.

(i) A global fit using only *TESS* data to check for inconsistencies arising from the *CHEOPS* data set.

(ii) A global fit using only *CHEOPS* data to check for inconsistencies arising from the *TESS* data set.

(iii) An independent analysis using the PATHOS code on all four *TESS* sectors.

The results of these tests, as presented in Fig. 3, confirm the final values of this work within 1σ.

Table 2 lists the most updated parameters for the TOI-561 planetary system.

4 IMPROVEMENT OF THE EPHEMERIDES

Thanks to the new data set above described, we improved the transit time precision and, the ephemerides of all four transiting planets. The most remarkable achievement has been to constrain the TOI-561 e period. In Fig. 4, we show the propagated error bar for the mid-transit time of each transiting planet orbiting TOI-561. We propagated the error bars until the first available transit after the date 2030 January 01 and compared our results with previous ephemerides from Lacedelli et al. (2022): TOI-561 b error bar at 2030 January 01 is 4.1 min (using Lacedelli et al. 2022 it would be 8.2 min), our propagated error is 50 per cent smaller; TOI-561 c error bar at 2030 January 01 is 13.2 min; TOI-561 d error bar at 2030 January 05 is 23.6 min; TOI-561 e error bar at 2030 February 17 is 19.2 min (in Lacedelli et al. 2022 it would be 13.0 d). The new uncertainty on transit time in 2030 is 974 times (99.9 per cent) smaller. This last improvement is fundamental for a future follow-up observation. With new *TESS* and *CHEOPS* data, the propagation of error bars for the mid-transit times has been significantly refined.

5 STABILITY ANALYSIS

The TOI-561 system hosts four confirmed planets (Table 2). In addition, RV data from HARPS-N has reported a 433 ± 20 d signal with

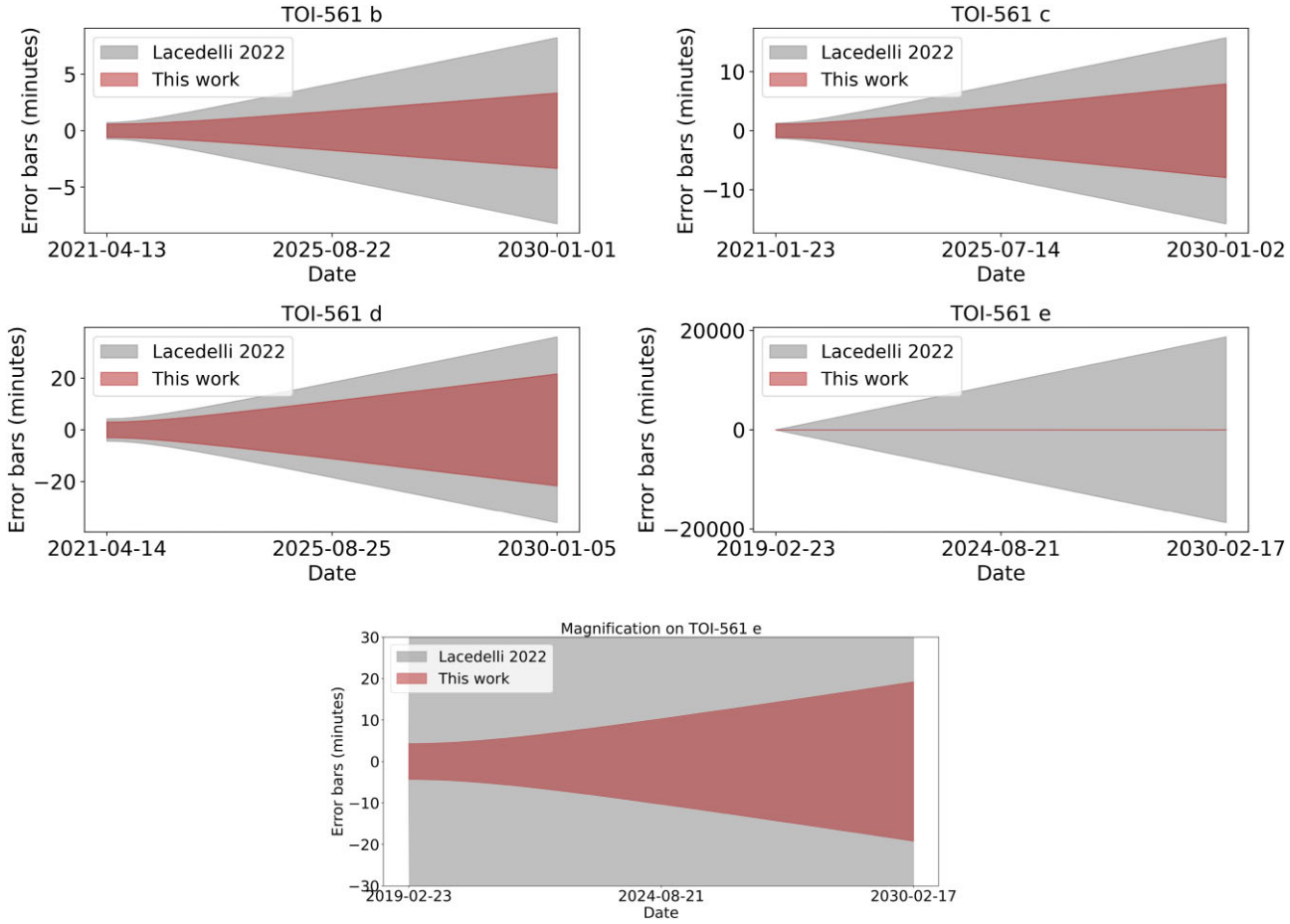

Figure 4. Upper part: error bars on the central transit time propagated until 2030 January 01. Note the improvement in mid-transit time for all planets. In particular, we present for the first time plausible ephemerides of planet TOI 561 e (with an error bar on mid-transit time 974 times lower than in Lacedelli et al. 2022, at 2030). This is important for possible follow-up of this planet, e.g. for TTV and TDV measurements. Bottom part: magnification of the planet TOI-561 e.

a semi-amplitude of about $K = 1.88 \pm 0.25$ m s^{-1} (Lacedelli et al. 2021), that may belong to a fifth external companion, corresponding to a planet-f with a mass around 19 $M_\oplus$.

To check the reliability of this additional planet, we performed a stability analysis of the five-planet system in a similar way as for other exoplanetary systems (eg. Correia et al. 2005, 2010). In Fig. 5, we numerically explore the stability of the system on a grid of initial conditions around the best fit (Table 2), by varying the orbital period and the eccentricity of the tentative planet-f, which is the most uncertain one. The whole figure covers the 1σ uncertainty that we have for the semi-amplitude K, and also 3σ for the orbital period. The black curve corresponds to $K = 1.88$ m s^{-1} and the best-fitting solution is marked with a dot.

Each initial condition was integrated for 10 000 yr, using the symplectic integrator SABAC4 (Laskar & Robutel 2001), with a step size of 2×10^{-5} yr and general relativity corrections. We then performed a frequency analysis (Laskar 1990, 1993) of the mean longitude of planet-f over two consecutive time intervals of 5000 yr, and determine the main frequency, n and n', respectively. The stability is measured by $\Delta = |1 - n'/n|$, which estimates the chaotic diffusion of the orbits. The results are reported in colour: orange and red represent strongly chaotic unstable trajectories, while cyan and blue give extremely stable quasi-periodic orbits on Gyr time-scales.

In Fig. 5, we observe that, despite we are analysing the outermost planet, several resonances are present that disturb the system. There is only a narrow blue stable region in the middle of the stability map, for orbital periods $P_f \approx 430 \pm 30$ d and eccentricities $e_f \lesssim 0.2$. Interestingly, this region is where the best-fitting solution from Table 2 lies. We conclude that the TOI-561 five-planet orbital solution is plausible from a dynamical point of view, and resilient to the uncertainties in the determination of the orbital period, eccentricity, and RV semi-amplitude of planet-f. Therefore, this analysis gives us an additional hint that the signal around 433 d reported in the HARPS-N data does have a planetary origin.

6 INTERNAL STRUCTURE MODELLING

As a next step, we applied the neural network-based internal structure modelling framework `plaNETic`[6] (Egger et al. 2024) to the four transiting planets in the TOI-561 system, using the updated planetary parameters listed in Table 2 as well as the stellar parameters from Lacedelli et al. (2022). `plaNETic` uses neural networks to replace the computationally intensive forward model in a Bayesian accept–reject sampling algorithm used to infer the internal structure of observed planets. The neural networks used in `plaNETic` were trained on the forward model of BICEPS (Bayesian Interior Characterization

[6]https://github.com/joannegger/plaNETic

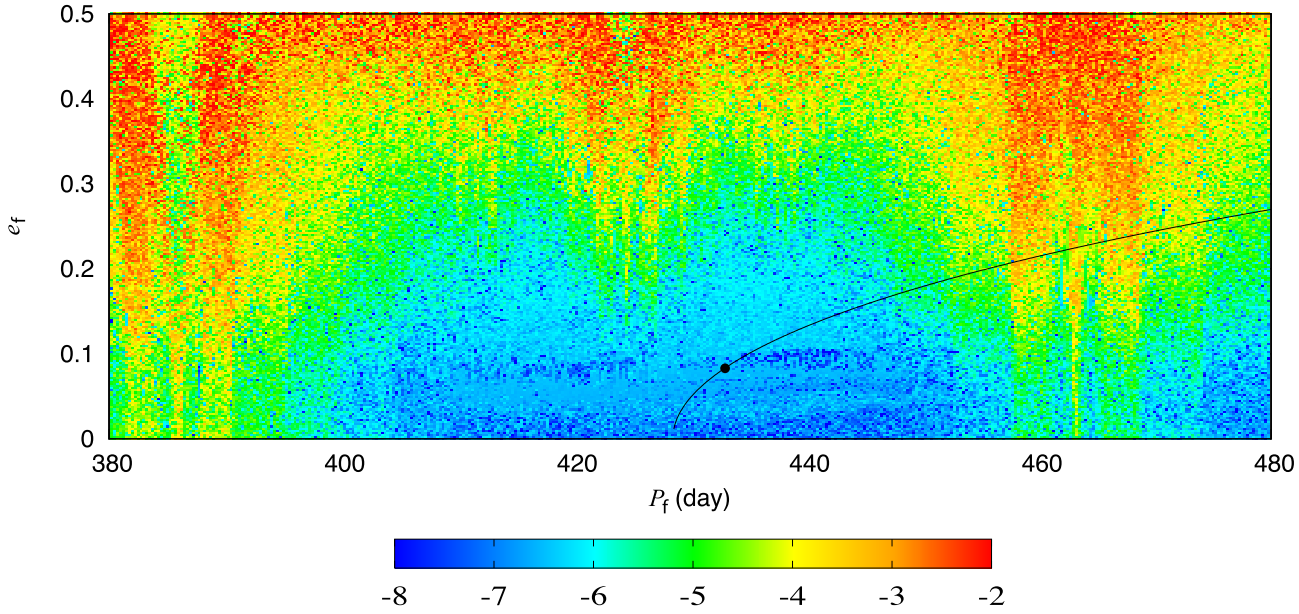

Figure 5. Stability analysis of the TOI-561 planetary system. For fixed initial conditions (Table 2), the parameter space of the system is explored by varying the orbital period and the eccentricity of planet-f. The step size is 0.25 d in the orbital period and 0.0025 in the eccentricity. For each initial condition, the system is integrated over 10 000 yr, and a stability indicator is calculated, which involved a frequency analysis of the mean longitude of the inner planet. The chaotic diffusion is measured by the variation in the main frequency. Red points correspond to highly unstable orbits, while blue points correspond to orbits that are likely to be stable on Gyr time-scales. The black curve corresponds to $K = 1.88\ \mathrm{m\,s^{-1}}$ and the black dot shows the values of the best-fitting solution (Table 2).

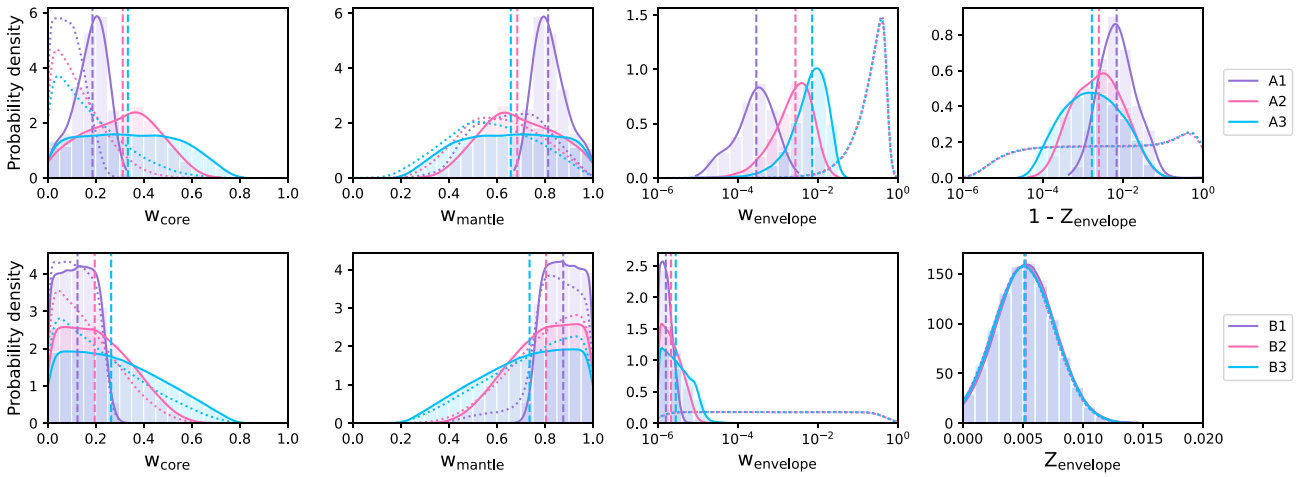

Figure 6. Results of the interior structure modelling for TOI-561 b using the `plaNETic` framework (Egger et al. 2024). The posterior distributions shown are for the mass fractions of an inner core (w_{core}), mantle (w_{mantle}), and envelope (w_{envelope}) in the planet as well as the mass fraction of water in the envelope (Z_{envelope}). We ran models assuming a formation scenario outside the iceline, leading to a water-rich composition (top row), as well as assuming a formation scenario inside the iceline and hence a water-poor composition (bottom row). For both water prior options, we ran three different models, once assuming the planet's Si/Mg/Fe ratios to match the ones of the star exactly (purple, option 1), once assuming the planet to be more iron-enriched (pink, option 2), and once using a free uniform prior for the planet's Si/Mg/Fe ratios (blue, option 3). The dotted lines depict the chosen priors, the dashed vertical lines the median values of the posterior distributions.

of ExoPlanetS , Haldemann et al. 2024) and include a much more physically accurate set of equations of state as well as an envelope of fully mixed H/He and water, in contrast to the interior models previously applied to these planets (Lacedelli et al. 2022; Patel et al. 2023), which used a condensed water layer with a separately modelled H/He envelope.

When inferring the internal structure of observed planets, the inherent degeneracy of the problem makes the resulting posteriors dependent on the chosen priors. To account for this effect, we ran a total of six different models per planet, with two different prior options for the water content of each planet and three prior options for a planet's Si/Mg/Fe ratios in relation to the stellar abundances measured for TOI-561 (see Lacedelli et al. 2022). For the water priors, we chose one option compatible with a scenario where the planet formed outside the iceline and is thus expected to be water-rich, as well as an option where the planet is expected to be water-poor. For the Si/Mg/Fe priors, we applied one prior assuming the planetary abundance ratios to match the stellar ones exactly (e.g. Thiabaud et al. 2015), one assuming the planet to be enriched in iron compared to the star (e.g. Adibekyan et al. 2021), and one modelling

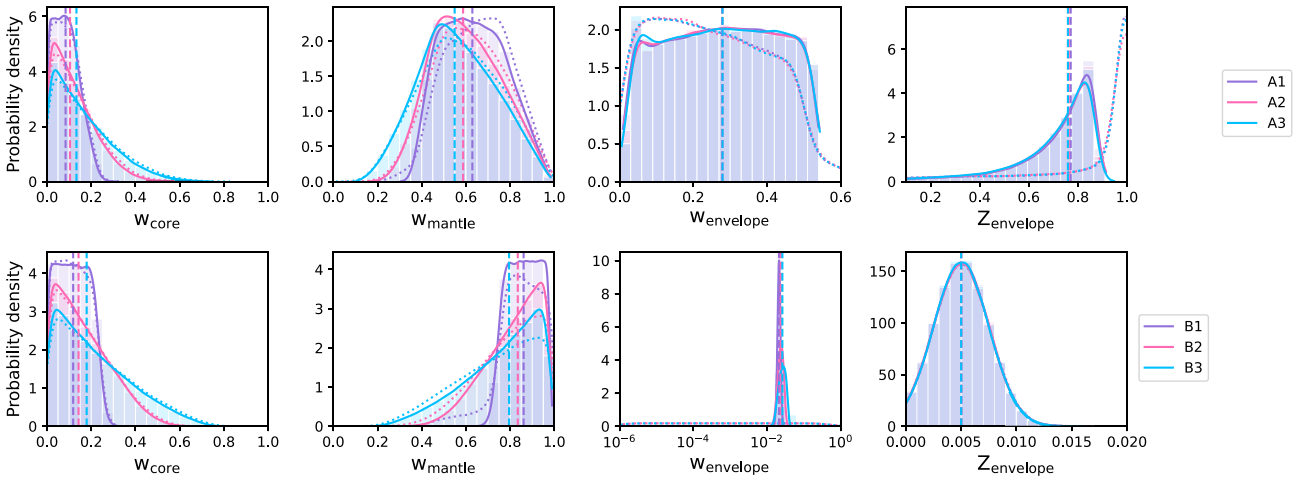

Figure 7. Same as Fig. 6, but for TOI-561 c.

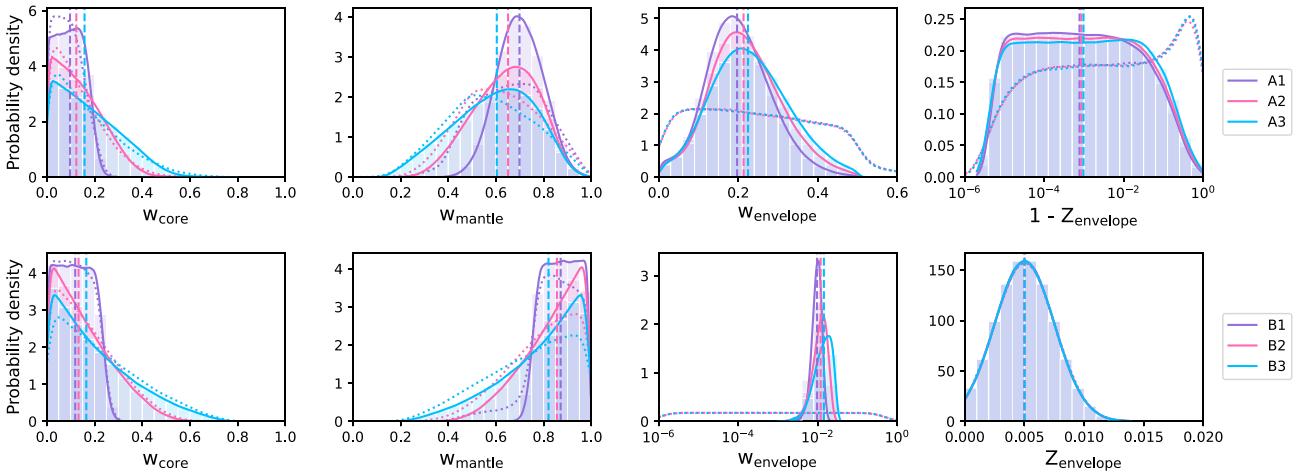

Figure 8. Same as Fig. 6, but for TOI-561 d.

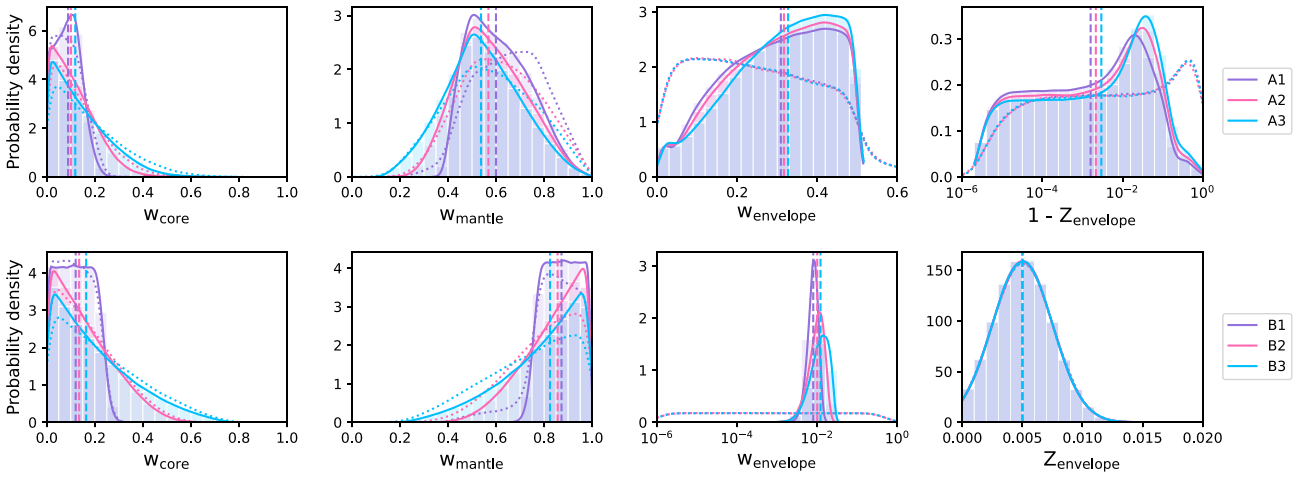

Figure 9. Same as Fig. 6, but for TOI-561 e.

the planet independently of the stellar Si/Mg/Fe ratios, with a uniform prior with an upper limit of 0.75 for iron. A more detailed description of these used priors and `plaNETic` in general can be found in Egger et al. (2024).

The most important resulting posteriors for TOI-561 b to e are visualized in Figs 6–9. Tables 3–6 summarize the median values and 1σ error intervals for all modelled internal structure parameters.For planet b, we find that the inferred envelope mass fractions are very

Table 3. Median and 1σ errors for the posterior distributions of the internal structure modelling for TOI-561 b.

Water prior	Formation outside iceline (water-rich)			Formation inside iceline (water-poor)		
Si/Mg/Fe prior [per cent]	Stellar (A1)	Iron-enriched (A2)	Free (A3)	Stellar (B1)	Iron-enriched (B2)	Free (B3)
$w_{\rm core}$	$18.7^{+5.6}_{-8.2}$	$31.3^{+14.4}_{-18.1}$	$33.4^{+22.6}_{-22.0}$	$12.4^{+8.2}_{-8.3}$	$19.6^{+16.4}_{-13.3}$	$26.4^{+23.2}_{-18.1}$
$w_{\rm mantle}$	$81.3^{+8.2}_{-5.7}$	$68.5^{+18.0}_{-14.6}$	$65.8^{+21.9}_{-22.6}$	$87.6^{+8.3}_{-8.2}$	$80.4^{+13.3}_{-16.4}$	$73.6^{+18.1}_{-23.2}$
$w_{\rm envelope}$	$0.03^{+0.05}_{-0.02}$	$0.27^{+0.38}_{-0.20}$	$0.71^{+0.85}_{-0.48}$	$\left(1.6^{+0.8}_{-0.4}\right)10^{-4}$	$\left(2.1^{+2.2}_{-0.9}\right)10^{-4}$	$\left(2.8^{+4.4}_{-1.4}\right)10^{-4}$
$Z_{\rm envelope}$	$99.3^{+0.4}_{-1.3}$	$99.8^{+0.2}_{-0.8}$	$99.8^{+0.1}_{-0.8}$	$0.5^{+0.2}_{-0.2}$	$0.5^{+0.2}_{-0.2}$	$0.5^{+0.2}_{-0.2}$
$x_{\rm Fe,core}$	$90.2^{+6.9}_{-6.2}$	$90.6^{+6.7}_{-6.7}$	$90.3^{+6.6}_{-6.3}$	$90.8^{+6.4}_{-6.6}$	$90.7^{+6.4}_{-6.6}$	$90.6^{+6.5}_{-6.6}$
$x_{\rm S,core}$	$9.8^{+6.2}_{-6.9}$	$9.4^{+6.7}_{-6.7}$	$9.7^{+6.3}_{-6.6}$	$9.2^{+6.6}_{-6.4}$	$9.3^{+6.6}_{-6.4}$	$9.4^{+6.6}_{-6.5}$
$x_{\rm Si,mantle}$	$44.7^{+6.5}_{-6.8}$	$32.4^{+9.4}_{-8.5}$	$21.1^{+19.8}_{-13.6}$	$40.5^{+6.0}_{-5.6}$	$36.8^{+7.7}_{-7.9}$	$27.7^{+28.0}_{-19.2}$
$x_{\rm Mg,mantle}$	$46.8^{+6.7}_{-6.9}$	$38.6^{+10.0}_{-9.3}$	$30.7^{+19.5}_{-16.0}$	$47.9^{+6.5}_{-6.2}$	$43.1^{+8.8}_{-9.3}$	$34.0^{+27.2}_{-22.1}$
$x_{\rm Fe,mantle}$	$7.7^{+7.5}_{-5.3}$	$28.3^{+16.5}_{-17.2}$	$46.2^{+16.8}_{-25.4}$	$11.5^{+6.8}_{-7.5}$	$18.7^{+15.7}_{-12.5}$	$30.9^{+23.8}_{-20.5}$

Table 4. Median and 1σ errors for the posterior distributions of the internal structure modelling for TOI-561 c.

Water prior	Formation outside iceline (water-rich)			Formation inside iceline (water-poor)		
Si/Mg/Fe prior [per cent]	Stellar (A1)	Iron-enriched (A2)	Free (A3)	Stellar (B1)	Iron-enriched (B2)	Free (B3)
$w_{\rm core}$	$8.4^{+6.5}_{-5.7}$	$10.4^{+11.8}_{-7.4}$	$13.3^{+16.5}_{-9.7}$	$11.8^{+8.1}_{-8.0}$	$14.2^{+15.5}_{-10.2}$	$17.9^{+21.3}_{-13.0}$
$w_{\rm mantle}$	$62.9^{+16.0}_{-14.9}$	$58.7^{+18.1}_{-14.7}$	$54.9^{+19.7}_{-16.5}$	$86.1^{+8.1}_{-8.2}$	$83.4^{+10.3}_{-15.8}$	$79.5^{+13.2}_{-21.7}$
$w_{\rm envelope}$	$27.8^{+17.1}_{-17.6}$	$27.9^{+17.1}_{-17.5}$	$27.9^{+17.1}_{-17.6}$	$2.1^{+0.2}_{-0.2}$	$2.4^{+0.4}_{-0.4}$	$2.6^{+0.7}_{-0.6}$
$Z_{\rm envelope}$	$77.1^{+7.8}_{-19.6}$	$76.3^{+8.2}_{-20.1}$	$75.9^{+8.2}_{-20.5}$	$0.5^{+0.2}_{-0.2}$	$0.5^{+0.2}_{-0.3}$	$0.5^{+0.2}_{-0.2}$
$x_{\rm Fe,core}$	$90.3^{+6.6}_{-6.4}$	$90.3^{+6.5}_{-6.4}$	$90.3^{+6.5}_{-6.3}$	$90.3^{+6.6}_{-6.4}$	$90.3^{+6.6}_{-6.4}$	$90.3^{+6.6}_{-6.3}$
$x_{\rm S,core}$	$9.7^{+6.4}_{-6.6}$	$9.7^{+6.4}_{-6.5}$	$9.7^{+6.3}_{-6.5}$	$9.7^{+6.4}_{-6.6}$	$9.7^{+6.4}_{-6.6}$	$9.7^{+6.3}_{-6.6}$
$x_{\rm Si,mantle}$	$40.5^{+6.0}_{-5.7}$	$38.1^{+7.6}_{-7.8}$	$33.2^{+29.4}_{-22.8}$	$40.5^{+6.0}_{-5.7}$	$38.3^{+7.5}_{-7.8}$	$33.9^{+29.2}_{-23.3}$
$x_{\rm Mg,mantle}$	$47.9^{+6.4}_{-6.1}$	$44.8^{+8.1}_{-9.1}$	$36.2^{+30.1}_{-24.6}$	$47.9^{+6.4}_{-6.1}$	$45.0^{+8.2}_{-9.0}$	$36.4^{+30.0}_{-24.7}$
$x_{\rm Fe,mantle}$	$11.5^{+6.7}_{-7.6}$	$15.5^{+15.4}_{-10.8}$	$22.0^{+24.0}_{-15.9}$	$11.6^{+6.7}_{-7.6}$	$15.1^{+15.2}_{-10.6}$	$21.3^{+23.6}_{-15.4}$

Table 5. Median and 1σ errors for the posterior distributions of the internal structure modelling for TOI-561 d.

Water prior	Formation outside iceline (water-rich)			Formation inside iceline (water-poor)		
Si/Mg/Fe prior [per cent]	Stellar (A1)	Iron-enriched (A2)	Free (A3)	Stellar (B1)	Iron-enriched (B2)	Free (B3)
$w_{\rm core}$	$9.7^{+6.5}_{-6.6}$	$12.4^{+12.0}_{-8.7}$	$15.8^{+16.4}_{-11.2}$	$11.9^{+8.2}_{-8.1}$	$13.3^{+15.4}_{-9.6}$	$16.6^{+21.4}_{-12.1}$
$w_{\rm mantle}$	$69.9^{+9.9}_{-9.5}$	$65.1^{+13.0}_{-15.3}$	$60.4^{+16.1}_{-19.8}$	$87.1^{+8.1}_{-8.2}$	$85.5^{+9.7}_{-15.7}$	$82.0^{+12.4}_{-21.8}$
$w_{\rm envelope}$	$19.7^{+8.6}_{-7.4}$	$21.3^{+9.7}_{-8.1}$	$22.4^{+10.5}_{-9.2}$	$1.0^{+0.3}_{-0.3}$	$1.2^{+0.5}_{-0.5}$	$1.4^{+0.8}_{-0.6}$
$Z_{\rm envelope}$	$99.9^{+0.1}_{-2.7}$	$99.9^{+0.1}_{-3.0}$	$99.9^{+0.1}_{-3.6}$	$0.5^{+0.2}_{-0.2}$	$0.5^{+0.2}_{-0.2}$	$0.5^{+0.2}_{-0.2}$
$x_{\rm Fe,core}$	$90.3^{+6.5}_{-6.4}$	$90.4^{+6.5}_{-6.4}$	$90.4^{+6.5}_{-6.4}$	$90.3^{+6.5}_{-6.4}$	$90.4^{+6.5}_{-6.4}$	$90.3^{+6.5}_{-6.4}$
$x_{\rm S,core}$	$9.7^{+6.4}_{-6.5}$	$9.6^{+6.4}_{-6.5}$	$9.6^{+6.4}_{-6.5}$	$9.7^{+6.4}_{-6.5}$	$9.6^{+6.4}_{-6.5}$	$9.7^{+6.4}_{-6.5}$
$x_{\rm Si,mantle}$	$40.6^{+6.0}_{-5.7}$	$38.1^{+7.5}_{-7.8}$	$32.9^{+30.1}_{-22.8}$	$40.6^{+6.0}_{-5.6}$	$38.8^{+7.4}_{-7.8}$	$35.9^{+29.4}_{-24.4}$
$x_{\rm Mg,mantle}$	$47.9^{+6.4}_{-6.2}$	$44.7^{+8.3}_{-8.9}$	$37.8^{+28.3}_{-24.8}$	$47.8^{+6.3}_{-6.1}$	$45.5^{+8.0}_{-9.0}$	$36.4^{+30.0}_{-24.8}$
$x_{\rm Fe,mantle}$	$11.4^{+6.8}_{-7.5}$	$15.7^{+15.0}_{-11.0}$	$21.4^{+22.5}_{-15.2}$	$11.6^{+6.7}_{-7.6}$	$13.9^{+15.2}_{-10.0}$	$19.3^{+23.7}_{-14.2}$

small for all chosen priors. If we assume a formation outside the iceline (case A), we end up with almost pure steam envelopes of <1 per cent. Conversely, for a formation scenario inside the iceline (case B), we infer largely H/He-dominated envelopes with mass fractions of the order of 10^{-6}, which would most likely have been evaporated. This is in agreement with the computations made in Patel et al. (2023).

If we assume that planets c, d, and e formed inside the iceline, we expect them to host almost pure H/He envelopes with mass fractions of around 2 per cent–3 per cent (c) and 1 per cent–2 per cent (d and e). If they formed inside the iceline, we expect their envelopes to be water-rich, with water mass fractions in the envelope of around 77^{+8}_{-20} per cent for planet c and almost pure water envelopes for planets d and e. The mass fractions of these water-dominated envelopes are expected to be around 28^{+17}_{-18} per cent for planet c, 21^{+10}_{-8} per cent for planet d, and 32^{+13}_{-15} per cent for planet e.

7 DISCUSSION AND CONCLUSIONS

With an age of $t_\star = 11.0^{+2.8}_{-3.5}$ Gyr (Lacedelli et al. 2022), TOI-561 is one of the oldest Milky Way disc stars known to have four confirmed planets, plus an additional fifth non-transiting candidate. TOI-561 system architecture has been controversial since its discovery. Weiss et al. (2021) interpreted the transit of TOI-561 e in *TESS* data as the transit of a planet with $\sim$ 16 d period. On the other hand, Lacedelli et al. (2021) suggested that the architecture of the TOI-561 system can be explained without the planet with a 16-d period. Later on, Lacedelli et al. (2022) found a 433 d signal in the HARPS-N RV data

Table 6. Median and 1σ errors for the posterior distributions of the internal structure modelling for TOI-561 e.

Water prior	Formation outside iceline (water-rich)			Formation inside iceline (water-poor)		
Si/Mg/Fe prior [per cent]	Stellar (A1)	Iron-enriched (A2)	Free (A3)	Stellar (B1)	Iron-enriched (B2)	Free (B3)
$w_{\rm core}$	$8.8^{+5.5}_{-5.8}$	$10.0^{+10.6}_{-7.1}$	$11.8^{+14.5}_{-8.6}$	$12.0^{+8.2}_{-8.2}$	$13.5^{+15.3}_{-9.7}$	$16.4^{+21.0}_{-12.0}$
$w_{\rm mantle}$	$59.9^{+15.2}_{-11.9}$	$56.8^{+16.4}_{-13.2}$	$53.7^{+17.0}_{-15.2}$	$87.2^{+8.2}_{-8.2}$	$85.6^{+9.8}_{-15.6}$	$82.4^{+12.2}_{-21.4}$
$w_{\rm envelope}$	$30.9^{+13.0}_{-15.4}$	$31.7^{+12.5}_{-15.4}$	$32.7^{+11.8}_{-15.2}$	$0.8^{+0.2}_{-0.2}$	$1.0^{+0.5}_{-0.4}$	$1.2^{+0.7}_{-0.6}$
$Z_{\rm envelope}$	$99.8^{+0.2}_{-3.2}$	$99.8^{+0.2}_{-4.3}$	$99.7^{+0.3}_{-5.2}$	$0.5^{+0.2}_{-0.2}$	$0.5^{+0.2}_{-0.2}$	$0.5^{+0.2}_{-0.2}$
$x_{\rm Fe,core}$	$90.1^{+6.7}_{-6.3}$	$90.2^{+6.7}_{-6.3}$	$90.3^{+6.6}_{-6.4}$	$90.3^{+6.5}_{-6.4}$	$90.4^{+6.5}_{-6.4}$	$90.3^{+6.5}_{-6.4}$
$x_{\rm S,core}$	$9.9^{+6.3}_{-6.7}$	$9.8^{+6.3}_{-6.7}$	$9.7^{+6.4}_{-6.6}$	$9.7^{+6.4}_{-6.5}$	$9.6^{+6.4}_{-6.5}$	$9.7^{+6.4}_{-6.5}$
$x_{\rm Si,mantle}$	$40.8^{+6.1}_{-5.7}$	$38.8^{+7.3}_{-7.8}$	$33.7^{+30.6}_{-23.5}$	$40.7^{+6.0}_{-5.7}$	$38.8^{+7.3}_{-7.8}$	$36.2^{+29.3}_{-24.5}$
$x_{\rm Mg,mantle}$	$48.2^{+6.3}_{-6.2}$	$45.8^{+8.0}_{-9.2}$	$37.1^{+31.4}_{-25.2}$	$47.8^{+6.3}_{-6.1}$	$45.5^{+8.0}_{-8.9}$	$36.6^{+30.0}_{-24.9}$
$x_{\rm Fe,mantle}$	$10.7^{+7.1}_{-7.1}$	$13.4^{+15.7}_{-9.6}$	$18.9^{+25.9}_{-14.0}$	$11.5^{+6.7}_{-7.5}$	$13.9^{+15.1}_{-10.0}$	$19.0^{+23.3}_{-13.9}$

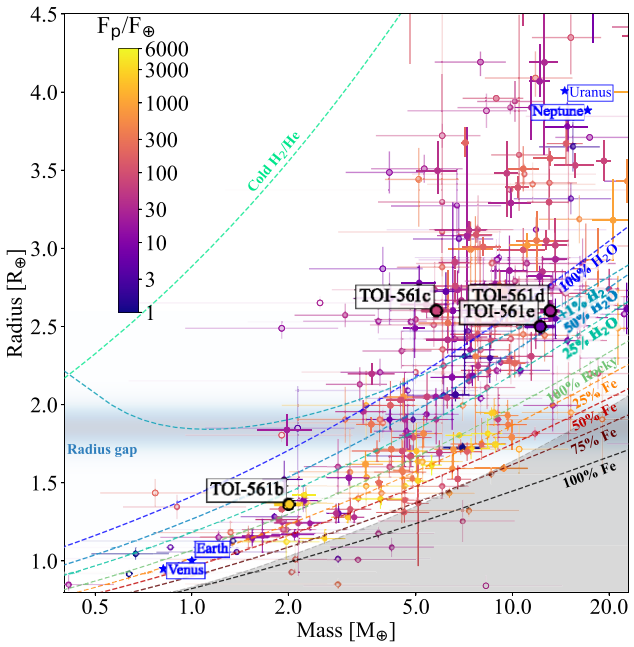

Figure 10. M–R diagram for TOI-561 system. The data are taken from the Extrasolar Planets Encyclopaedia catalogue (http://exoplanet.eu/catalog/) as of 2024 May. The TOI-561 planets are labelled and updated with the analysis in the current work. The theoretical M−R relationship as a function of the chemical composition (Zeng et al. 2019) are shown in dashed coloured lines. The shaded grey region represents the forbidden region predicted by collisional stripping (Marcus et al. 2010).

that could be planetary in nature. TOI-561 e, originally inferred from *TESS* Sector 8 and HARPS-N RV data, has now been confirmed with new *TESS*+*CHEOPS* light curves, definitely fixing the architecture of the planetary system. The masses of all planets have been measured at ~ 10 per cent precision, while the radii have been determined with ~ 2 per cent precision.

New *CHEOPS* and *TESS* data allowed us to estimate the density of the planets, including TOI-561 e, with unprecedented precision, and to properly place all the planets in the mass–radius (M–R) diagram (Fig. 10). The system includes one of the lowest density USP super-Earth TOI-561 b with a density $\rho_p = 4.3 \pm 0.6\,{\rm g\,cm^{-3}}$. Our analysis refined the radius and the period of the outer transiting planet TOI-561 e, which is confirmed to be a mini-Neptune with a radius of $R_p = 2.49 \pm 0.05\,{\rm R_\oplus}$ and a mass of $M_p = 12.4 \pm 1.4\,{\rm M_\oplus}$, with stellar irradiation of $4.89 \pm 0.16\,{\rm S_\oplus}$ and an equilibrium temperature of 414 ± 3K, assuming a bond albedo $A_B = 0$.

The new observational data allowed us to improve the ephemerides of all planets, in particular we obtained a 99.9 per cent reduction of the uncertainty on TOI-561 e ephemerides. TOI-561 e is one of a few good candidates for exomoon search. With a period of about 77 d, it is above the period threshold of 60 d, suggested by Alvarado-Montes, Zuluaga & Sucerquia (2017), below which the exomoon would collide with the planet. As described in Ehrenreich et al. (2023), the observation aimed to search for exomoon should be centred on the transit of the planet, and should span the time equivalent of the Hill radius of the planet, because a stable exomoon is expected to lie within the planet Hill sphere (Domingos, Winter & Yokoyama 2006). For this reason, the improvement we obtained on the linear ephemerides of planet e has a crucial importance for the planning and scheduling of future observations.

Finally, the stability analysis performed in this paper demonstrated the long-term stability of the outer candidate TOI-561 f, validating even further its existence. This paper presents a definitive characterization of the exoplanet system of TOI-561, with confirmation of the five planets and improvement of ephemerides, orbital, and physical parameters, thanks to the new data from *CHEOPS* and *TESS*. Specifically, the great improvement in transit-timing precision and the fine-tuning of internal structure models underlines the relevance of TOI-561 for ongoing and future studies.

ACKNOWLEDGEMENTS

CHEOPS is an ESA mission in partnership with Switzerland with important contributions to the payload and the ground segment from Austria, Belgium, France, Germany, Hungary, Italy, Portugal, Spain, Sweden, and the United Kingdom. The *CHEOPS* Consortium would like to gratefully acknowledge the support received by all the agencies, offices, universities, and industries involved. Their flexibility and willingness to explore new approaches were essential to the success of this mission. *CHEOPS* data analysed in this article will be made available in the *CHEOPS* mission archive (https://cheops.unige.ch/archive_browser/). LBo, GBr, VNa, IPa, GPi, RRa, GSc, VSi, and TZi acknowledge support from *CHEOPS*ASI-INAF agreement no. 2019-29-HH.0. TZi acknowledges NVIDIA Academic Hardware Grant Program for the use of the Titan V GPU card and the Italian MUR Departments of Excellence grant 2023–2027 'Quantum Frontiers'. This work has been carried out within the framework of the NCCR PlanetS supported by the Swiss National Science Foundation under grants 51NF40_182901 and 51NF40_205606. ACMC acknowledges

support from the FCT, Portugal, through the CFisUC projects UIDB/04564/2020 and UIDP/04564/2020, with DOI identifiers 10.54499/UIDB/04564/2020 and 10.54499/UIDP/04564/2020, respectively. AC, AD, BE, KG, and JK acknowledge their role as ESA-appointed *CHEOPS* Science Team Members. AS acknowledges support from the Swiss Space Office through the ESA PRODEX program. SGS acknowledge support from FCT through FCT contract no. CEECIND/00826/2018 and POPH/FSE (EC). The Portuguese team thanks the Portuguese Space Agency for the provision of financial support in the framework of the PRODEX Programme of the European Space Agency (ESA) under contract no.4000142255. PM acknowledges support from STFC research grant no. ST/R000638/1. TWi acknowledges support from the UKSA and the University of Warwick. YAl acknowledges support from the Swiss National Science Foundation (SNSF) under grant 200020_192038. NCSa acknowledges funding by the European Union (ERC, FIERCE, 101052347). Views and opinions expressed are however those of the author(s) only and do not necessarily reflect those of the European Union or the European Research Council. Neither the European Union nor the granting authority can be held responsible for them. LMS gratefully acknowledges financial support from the CRT foundation under grant no. 2018.2323 'Gaseous or rocky? Unveiling the nature of small worlds'. We acknowledge financial support from the Agencia Estatal de Investigación of the Ministerio de Ciencia e Innovación MCIN/AEI/10.13039/501100011033 and the ERDF 'A way of making Europe' through projects PID2019-107061GB-C61, PID2019-107061GB-C66, PID2021-125627OB-C31, and PID2021-125627OB-C32, from the Centre of Excellence 'Severo Ochoa' award to the Instituto de Astrofísica de Canarias (CEX2019-000920-S), from the Centre of Excellence 'María de Maeztu' award to the Institut de Ciències de l'Espai (CEX2020-001058-M), and from the Generalitat de Catalunya/CERCA programme. We acknowledge financial support from the Agencia Estatal de Investigación of the Ministerio de Ciencia e Innovación MCIN/AEI/10.13039/501100011033 and the ERDF 'A way of making Europe' through projects PID2019-107061GB-C61, PID2019-107061GB-C66, PID2021-125627OB-C31, and PID2021-125627OB-C32, from the Centre of Excellence 'Severo Ochoa' award to the Instituto de Astrofísica de Canarias (CEX2019-000920-S), from the Centre of Excellence 'María de Maeztu' award to the Institut de Ciències de l'Espai (CEX2020-001058-M), and from the Generalitat de Catalunya/CERCA programme. SCCB acknowledges support from FCT through FCT contracts no. IF/01312/2014/CP1215/CT0004. ABr was supported by the SNSA. CB acknowledges support from the Swiss Space Office through the ESA PRODEX program. ACC acknowledges support from STFC consolidated grant no. ST/V000861/1, and UKSA grant no. ST/X002217/1. PEC is funded by the Austrian Science Fund (FWF) Erwin Schroedinger Fellowship, program J4595-N. This project was supported by the CNES. This work was supported by FCT – Fundação para a Ciência e a Tecnologia through national funds and by FEDER through COMPETE2020 through the research grants UIDB/04434/2020, UIDP/04434/2020, and 2022.06962.PTDC. ODSD is supported in the form of work contract (DL 57/2016/CP1364/CT0004) funded by national funds through FCT. B-OD acknowledges support from the Swiss State Secretariat for Education, Research and Innovation (SERI) under contract no. MB22.00046. AC, AD, BE, KG, and JK acknowledge their role as ESA-appointed *CHEOPS* Science Team Members. This project has received funding from the Swiss National Science Foundation for project 200021_200726. It has also been carried out within the framework of the National Centre of Competence in Research PlanetS supported by the Swiss National Science Foundation under grant 51NF40_205606. The authors acknowledge the financial support of the SNSF. MF and CMP gratefully acknowledge the support of the Swedish National Space Agency (DNR 65/19, 174/18). DG gratefully acknowledges financial support from the CRT foundation under grant no. 2018.2323' 'Gaseousor rocky? Unveiling the nature of small worlds'. MG is an F.R.S.-FNRS Senior Research Associate. MNG is the ESA *CHEOPS* Project Scientist and Mission Representative, and as such also responsible for the Guest Observers (GO) Programme. MNG does not relay proprietary information between the GO and Guaranteed Time Observation (GTO) Programmes, and does not decide on the definition and target selection of the GTO Programme. CHe acknowledges support from the European Union H2020-MSCA-ITN-2019 under grant agreement no. 860470 (CHAMELEON). KGI is the ESA *CHEOPS* Project Scientist and is responsible for the ESA *CHEOPS* Guest Observers Programme. She does not participate in, or contribute to, the definition of the Guaranteed Time Programme of the *CHEOPS* mission through which observations described in this paper have been taken, nor to any aspect of target selection for the programme. KWFL was supported by Deutsche Forschungsgemeinschaft grants RA714/14-1 within the DFG Schwerpunkt SPP 1992, Exploring the Diversity of Extrasolar Planets. This work was granted access to the HPC resources of MesoPSL financed by the Region Ile de France and the project Equip@Meso (reference ANR-10-EQPX-29-01) of the programme Investissements d'Avenir supervised by the Agence Nationale pour la Recherche. ML acknowledges support of the Swiss National Science Foundation under grant no. PCEFP2_194576. This work was also partially supported by a grant from the Simons Foundation (PI: Queloz, grant no. 327127). GyMSz acknowledges the support of the Hungarian National Research, Development and Innovation Office (NKFIH) grant K-125015, a PRODEX Experiment agreement no. 4000137122, the Lendület LP2018-7/2021 grant of the Hungarian Academy of Science and the support of the city of Szombathely. VVG is an F.R.S-FNRS Research Associate. JV acknowledges support from the Swiss National Science Foundation (SNSF) under grant PZ00P2_208945. NAW acknowledges UKSA grant ST/R004838/1. *CHEOPS* Program MR. Improve-CHESS ID: 0031.

DATA AVAILABILITY

HARPS-N observations and data products are available through the Data and Analysis Center for Exoplanets (DACE) at https://dace.unige.ch/. *TESS* data products can be accessed through the official NASA website https://heasarc.gsfc.nasa.gov/docs/tess/data-access.html. All underlying data are available either in the appendix/online supporting information or will be available via VizieR at CDS.

REFERENCES

Adibekyan V. et al., 2021, Science, 374, 330
Alvarado-Montes J. A., Zuluaga J. I., Sucerquia M., 2017, MNRAS, 471, 3019
Bashi D., Zucker S., 2021, MNRAS, 510, 3449
Benz W. et al., 2021, Exp. Astron., 51, 109
Brinkman C. et al., 2022, AJ, 165, 88
Claret A., 2017, A&A, 600, A30
Claret A., 2021, Res. Notes Am. Astron. Soc., 5, 13
Correia A. C. M., Udry S., Mayor M., Laskar J., Naef D., Pepe F., Queloz D., Santos N. C., 2005, A&A, 440, 751
Correia A. C. M. et al., 2010, A&A, 511, A21
Cosentino R. et al., 2014, in Ramsay S. K., McLean I. S., Takami H.eds, Proc. SPIE Conf. Ser., Vol. 9147, Ground-based and Airborne Instrumentation for Astronomy V, Optical Engineering, p. 91478C

Domingos R. C., Winter O. C., Yokoyama T., 2006, MNRAS, 373, 1227
Egger J. A. et al., 2024, A&A, 688, A223
Ehrenreich D. et al., 2023, A&A, 671, A154
Espinoza N., Kossakowski D., Brahm R., 2019, MNRAS, 490, 2262
Fausnaugh M. M. et al., 2021, ApJ, 908, 51
Foreman-Mackey D., Hogg D. W., Lang D., Goodman J., 2013, PASP, 125, 306
Fortier A. et al., 2024, A&A, 687, A302
Haldemann J., Dorn C., Venturini J., Alibert Y., Benz W., 2024, A&A, 681, A96
Hippke M., David T. J., Mulders G. D., Heller R., 2019, AJ, 158, 143
Hoyer S., Guterman P., Demangeon O., Sousa S. G., Deleuil M., Meunier J. C., Benz W., 2020, A&A, 635, A24
Kipping D. M., 2013, MNRAS, 435, 2152
Lacedelli G. et al., 2021, MNRAS, 501, 4148
Lacedelli G. et al., 2022, MNRAS, 511, 4551
Laskar J., 1990, Icarus, 88, 266
Laskar J., 1993, Phys. D Nonlinear Phenom., 67, 257
Laskar J., Robutel P., 2001, Celest. Mech. Dyn. Astron., 80, 39
Malavolta L. et al., 2016, A&A, 588, A118
Malavolta L. et al., 2018, AJ, 155, 107
Marcus R. A., Sasselov D., Hernquist L., Stewart S. T., 2010, ApJ, 712, L73
Maxted P. F. L. et al., 2021, MNRAS, 514, 77
Mosteller F., Tukey J. W., 1977, Data Analysis and Regression. A Second Course in Statistics, Addison-Wesley , University of Michigan
Nardiello D., 2020, MNRAS, 498, 5972
Nardiello D. et al., 2019, MNRAS, 490, 3806
Nardiello D. et al., 2020, MNRAS, 495, 4924
Nardiello D. et al., 2021, MNRAS, 505, 3767
Newville M., Stensitzki T., Allen D. B., Ingargiola A., 2014, LMFIT: Non-Linear Least-Square Minimization and Curve-Fitting for Python. Zenodo, doi:10.5281/zenodo.11813
Parviainen H., 2016, PyDE: v1.5, Zenodo, https://doi.org/10.5281/zenodo.45602
Patel J. A. et al., 2023, A&A, 679, A92
Ricker G. R. et al., 2015, J. Astron. Telesc. Instrum. Syst., 1, 014003
Thiabaud A., Marboeuf U., Alibert Y., Leya I., Mezger K., 2015, A&A, 580, A30
Vogt S. S., Keane M. J., 1993, American Astronomical Society Meeting Abstracts, #11.01
Weiss L. M. et al., 2021, AJ, 161, 56
Zeng L. et al., 2019, Proc. Natl. Acad. Sci., 116, 9723

[1]*Dipartimento di Fisica e Astronomia 'Galileo Galilei', Università degli Studi di Padova, Vicolo dell'Osservatorio 3, I-35122 Padova, Italy*
[2]*INAF, Osservatorio Astronomico di Padova, Vicolo dell'Osservatorio 5, I-35122 Padova, Italy*
[3]*Weltraumforschung und Planetologie, Physikalisches Institut, University of Bern, Gesellschaftsstrasse 6, CH-3012 Bern, Switzerland*
[4]*CFisUC, Departamento de Física, Universidade de Coimbra, P-3004-516 Coimbra, Portugal*
[5]*Center for Space and Habitability, University of Bern, Gesellschaftsstrasse 6, CH-3012 Bern, Switzerland*
[6]*Department of Astronomy, Stockholm University, AlbaNova University Center, SE-10691 Stockholm, Sweden*
[7]*Instituto de Astrofisica e Ciencias do Espaco, Universidade do Porto, CAUP, Rua das Estrelas, P-4150-762 Porto, Portugal*
[8]*Astrophysics Group, Lennard Jones Building, Keele University, Staffordshire ST5 5BG, UK*
[9]*Department of Physics, University of Warwick, Gibbet Hill Road, Coventry CV4 7AL, UK*
[10]*Space Research Institute, Austrian Academy of Sciences, Schmiedlstrasse 6, A-8042 Graz, Austria*
[11]*Department of Astronomy & Astrophysics, University of Chicago, Chicago, IL 60637, USA*
[12]*Departamento de Fisica e Astronomia, Faculdade de Ciencias, Universidade do Porto, Rua do Campo Alegre, P-4169-007 Porto, Portugal*
[13]*Cavendish Laboratory, JJ Thomson Avenue, Cambridge CB30HE, UK*
[14]*Institute of Planetary Research, German Aerospace Center (DLR), Rutherfordstrasse 2, D-12489 Berlin, Germany*
[15]*Observatoire Astronomique de l'Université de Genève, Chemin Pegasi 51, CH-1290 Versoix, Switzerland*
[16]*Instituto de Astrofísica de Canarias, Vía Láctea s/n, E-38200 La Laguna, Tenerife, Spain*
[17]*Departamento de Astrofísica, Universidad de La Laguna, Astrofísico Francisco Sanchez s/n, E-38206 La Laguna, Tenerife, Spain*
[18]*Admatis, 5. Kandó Kálmán Street, 3534 Miskolc, Hungary*
[19]*Departamento de Astrofísica, Centro de Astrobiología (CSIC-INTA), ESAC Campus, E-28692 Villanueva de la Cañada (Madrid),Spain*
[20]*Centre for Exoplanet Science, SUPA School of Physics and Astronomy, University of St Andrews, North Haugh, St Andrews KY16 9SS, UK*
[21]*INAF, Osservatorio Astrofisico di Torino, Via Osservatorio, 20, I-10025 Pino Torinese To, Italy*
[22]*Centre for Mathematical Sciences, Lund University, Box 118, SE-221 00 Lund, Sweden*
[23]*LAM, Aix Marseille University, CNRS, CNES, 38 rue Frédéric Joliot-Curie, F-13388 Marseille, France*
[24]*ELTE Gothard Astrophysical Observatory, 9700 Szombathely, Szent Imre h. u. 112, Hungary*
[25]*SRON Netherlands Institute for Space Research, Niels Bohrweg 4, NL-2333 CA Leiden, the Netherlands*
[26]*Centre Vie dans l'Univers, Faculté des Sciences, Université de Genève, Quai Ernest-Ansermet 30, CH-1211 Genève 4, Switzerland*
[27]*Leiden Observatory, University of Leiden, PO Box 9513, NL-2300 RA Leiden, the Netherlands*
[28]*Department of Space, Earth and Environment, Chalmers University of Technology, Onsala Space Observatory, SE-439 92 Onsala, Sweden*
[29]*Dipartimento di Fisica, Università degli Studi di Torino, via Pietro Giuria 1, I-10125, Torino, Italy*
[30]*Department of Physics, National and Kapodistrian University of Athens, University Campus, Zografos GR-157 84, Athens, Greece*
[31]*Astrobiology Research Unit, Université de Liège, Allée du 6 Août 19C, B-4000 Liège, Belgium*
[32]*Department of Astrophysics, University of Vienna, Türkenschanzstrasse 17, A-1180 Vienna, Austria*
[33]*European Space Agency (ESA), European Space Research and Technology Centre (ESTEC), Keplerlaan 1, NL-2201 AZ Noordwijk, the Netherlands*
[34]*Institute for Theoretical Physics and Computational Physics, Graz University of Technology, Petersgasse 16, A-8010 Graz, Austria*
[35]*Konkoly Observatory, Research Centre for Astronomy and Earth Sciences, 1121 Budapest, Konkoly Thege Miklós út 15-17, Hungary*
[36]*ELTE Eötvös Loránd University, Institute of Physics, Pázmány Péter sétány 1/A, 1117 Budapest, Hungary*
[37]*Lund Observatory, Division of Astrophysics, Department of Physics, Lund University, Box 118, SE-22100 Lund, Sweden*
[38]*IMCCE, UMR8028 CNRS, Observatoire de Paris, PSL University, Sorbonne Universites, 77 av. Denfert-Rochereau, F-75014 Paris, France*
[39]*Institut d'Astrophysique de Paris, , France*
[40]*Dipartimento di Fisica, Università di Trento, Via Sommarive 14, 38123, Povo, Trento, Italy*
[41]*INAF, Osservatorio Astrofisico di Catania, Via S. Sofia 78, I-95123 Catania, Italy*
[42]*Institute of Optical Sensor Systems, German Aerospace Center (DLR), Rutherfordstrasse 2, D-12489 Berlin, Germany*
[43]*Department of Astrophysical Sciences, Princeton University, Princeton, NJ 08544, USA*
[44]*Department of Physics, ETH Zurich, Wolfgang-Pauli-Strasse 2, CH-8093 Zurich, Switzerland*
[45]*Institut fuer Geologische Wissenschaften, Freie Universitaet Berlin, Maltheserstrasse 74-100, D-12249 Berlin, Germany*
[46]*Institut de Ciencies de l'Espai (ICE, CSIC), Campus UAB, Can Magrans s/n, E-08193 Bellaterra, Spain*
[47]*Institut d'Estudis Espacials de Catalunya (IEEC), E-08860 Castelldefels (Barcelona), Spain*

[48]*INAF – Osservatorio Astrofisico di Catania,Oss. Astr. Catania,via S. Sofia 78, I-95123 Catania, Italy*
[49]*Space Sciences, Technologies and Astrophysics Research (STAR) Institute, Université de Liège, Allée du 6 Août 19C, B-4000 Liège, Belgium*
[50]*HUN-REN-ELTE Exoplanet Research Group, Szent Imre h. u. 112., Szombathely, H-9700, Hungary*

This paper has been typeset from a TEX/LATEX file prepared by the author.